Monthly Notices
of the
ROYAL ASTRONOMICAL SOCIETY

MNRAS **471,** 3878–3887 (2017)
Advance Access publication 2017 July 25

doi:10.1093/mnras/stx1865

The 2016 super-Eddington outburst of SMC X-3: X-ray and optical properties and system parameters

L. J. Townsend,[1]★ J. A. Kennea,[2] M. J. Coe,[3] V. A. McBride,[1,4] D. A. H. Buckley,[4] P. A. Evans[5] and A. Udalski[6]

[1]*Department of Astronomy, University of Cape Town, Private Bag X3, Rondebosch, 7701, South Africa*
[2]*Department of Astronomy and Astrophysics, Pennsylvania State University, 525 Davey Lab, University Park, PA 16802, USA*
[3]*Physics and Astronomy, University of Southampton, Southampton SO17 1BJ, UK*
[4]*South African Astronomical Observatory, PO Box 9, Observatory 7935, South Africa*
[5]*Department of Physics and Astronomy, University of Leicester, Leicester LE1 7RH, UK*
[6]*Warsaw University Observatory, Aleje Ujazdowskie 4, PL-00-478 Warsaw, Poland*

Accepted 2017 July 20. Received 2017 July 20; in original form 2017 January 10

ABSTRACT

On 2016 July 30 (MJD 57599), observations of the Small Magellanic Cloud by *Swift*/XRT found an increase in X-ray counts coming from a position consistent with the Be/X-ray binary pulsar SMC X-3. Follow-up observations on 2016 August 3 (MJD 57603) and 2016 August 10 (MJD 57610) revealed a rapidly increasing count rate and confirmed the onset of a new X-ray outburst from the system. Further monitoring by *Swift* began to uncover the enormity of the outburst, which peaked at 1.2×10^{39} erg s^{-1} on 2016 August 25 (MJD 57625). The system then began a gradual decline in flux that was still continuing over 5 months after the initial detection. We explore the X-ray and optical behaviour of SMC X-3 between 2016 July 30 and 2016 December 18 during this super-Eddington outburst. We apply a binary model to the spin-period evolution that takes into account the complex accretion changes over the outburst, to solve for the orbital parameters. Our results show SMC X-3 to be a system with a moderately low eccentricity amongst the Be/X-ray binary systems and to have a dynamically determined orbital period statistically consistent with the prominent period measured in the OGLE optical light curve. Our optical and X-ray derived ephemerides show that the peak in optical flux occurs roughly 6 d after periastron. The measured increase in *I*-band flux from the counterpart during the outburst is reflected in the measured equivalent width of the H_α line emission, though the H_α emission itself seems variable on sub-day time-scales, possibly due to the NS interacting with an inhomogeneous disc.

Key words: ephemerides – stars: emission-line, Be – Magellanic Clouds – X-rays: binaries.

1 INTRODUCTION

High-mass X-ray binaries (HMXBs) comprise a compact object in orbit around an early-type star. Continuous or transient interactions between the two bodies cause X-rays to be produced on a range of time-scales and across a large range in luminosity. They have been observed in large numbers in the Milky Way and Magellanic Clouds, thanks to continuous monitoring from all-sky X-ray detectors and more focused surveys from several X-ray telescopes. The Small Magellanic Cloud (SMC) in particular is an exceptional host galaxy when it comes to HMXBs, with 121 high-confidence HMXB systems now known (Haberl & Sturm 2016). This is higher than the known population of HMXBs in the Milky Way, despite the significantly lower mass of the SMC. The most probable reason for this is recent (∼400 Myr ago) bursts of star formation resulting in large numbers of massive, young stars, and the low line-of-sight extinction to the Magellanic Clouds. Work in this area is well documented (e.g. Dray 2006; Antoniou et al. 2010), though the details are beyond the scope of this paper. Of these 121 systems, 64 are confirmed pulsars (Haberl & Sturm 2016; Vasilopoulos et al. 2016). A detailed account of the optical and infra-red properties of this group of pulsating systems can be found in Coe & Kirk (2015).

HMXBs can be divided into three main groups: supergiant X-ray binaries (SGXRBs), Be-X/ray binaries (BeXRBs) and supergiant fast X-ray transients (SFXTs). As the focus of this paper is the well known BeXRB pulsar SMC X-3, we follow with a brief summary of this type of system. Recent good reviews of each type of HMXB system can be found in Reig (2011) and Walter et al. (2015). BeXRBs comprise an early-type main-sequence or giant star that

★ E-mail: townsend@ast.uct.ac.za

shows, or has shown, emission in the Balmer series. The majority of compact objects in these systems are neutron stars, though many remain unidentified. There is only one system with a confirmed black hole (Casares et al. 2014). They are the most numerous group of HMXBs known and show significant variability in both time and luminosity, due to the wide range of observed binary parameters and the intrinsic variability of the Be star. In some circumstances, these systems can produce X-ray emission in excess of the Eddington limit for a nominal mass neutron star.

SMC X-3 was the third X-ray source to be discovered in the SMC, by the SAS 3 satellite in 1977 (Li, Jernigan & Clark 1977; Clark et al. 1978). In 2002, the *Rossi X-ray Timing Explorer (RXTE)* discovered a new pulsating X-ray source in the SMC, with a period of roughly 7.8 s (Corbet et al. 2003). Those authors detected this period several times during the following year, leading to the identification of a probable orbital period of ∼45 d. It was not until 2004 that the association between this X-ray pulsar and SMC X-3 was made. Edge et al. (2004) used an archival *Chandra* observation to precisely locate SMC X-3 and determine a 7.78 s period in the light curve. The observation was made 3 d before a *RXTE* detection of the 7.8 s period, confirming the association of the *RXTE* and *Chandra* sources. The precise *Chandra* position from this work (00h52m05.7s, -72d26m05s (J2000.0), uncertainty 0.6 arcsec) was consistent with the position of the originally proposed optical counterpart to SMC X-3 (van Paradijs et al. 1977; Crampton, Hutchings & Cowley 1978). An optical modulation in long-term MACHO photometry was found at 44.86 d by Cowley & Schmidtke (2004). The authors note that this is very close to the X-ray period determined by Corbet et al. (2003) and conclude that it represents the binary period of the system. Edge (2005) also found a significant modulation in long-term OGLE photometry at 44.8 d, during a phase of apparent X-ray quiescence. The long-term *RXTE* light curve of SMC X-3 is presented in Galache et al. (2008). The authors determine a full X-ray ephemeris of MJD 52,250.9 ± 1.4 + 44.92n ± 0.06 d, where 44.92 d is the prominent modulation in the light curve and agrees well with the optically derived periods. In addition, the light curve seems to show distinct periods of X-ray activity lasting between ∼200–400 d and separated by ∼1000 d. Intriguingly, the authors note that there appears to be evidence of weak X-ray emission at apastron in the folded light curve and that the overall trend in the light curve is a spin-down of the pulsar. The *RXTE* light curve and spin period evolution are discussed in more detail in Section 2.3. Schmidtke, Cowley & Udalski (2013) refine the optical period to 44.94 ± 0.02 d using more recent OGLE III data. The authors also observe a dip in the folded light curve immediately before optical maximum, when the system is in an optically bright state. Finally, the spectral type of the counterpart was determined to be B1–1.5 IV–V (McBride et al. 2008).

Here, we describe the recent super-Eddington outburst of SMC X-3. The original detection of the outburst was made by *MAXI* on 2016 August 8 (Negoro et al. 2016), although they were unable to identify conclusively that it was SMC X-3. The association was confirmed from multiple detections of the outburst by *Swift* (Kennea et al. 2016). The outburst was estimated to begin sometime between 2016 July 16 and 2016 July 30 based on *Swift/XRT* observations of the SMC and was still ongoing over 5 months after this initial detection. After submission of this manuscript, further analysis of this outburst was presented in Weng et al. (2017) and Tsygankov et al. (2017). Those authors independently derive binary solutions for SMC X-3, which we compare to our results. They also present determinations of the magnetic field strength of the neutron star, which are slightly inconsistent with each other. The magnetic field

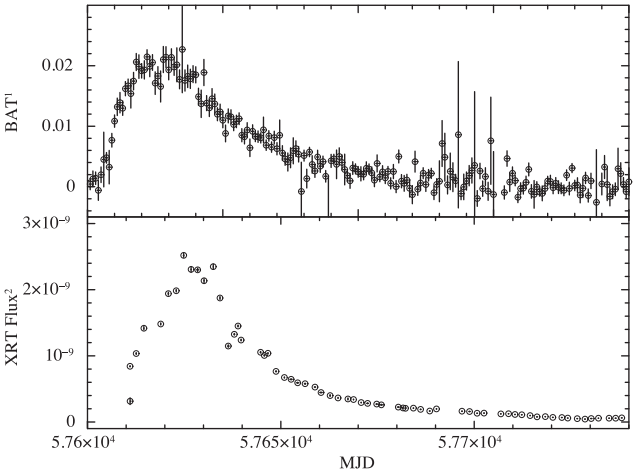

Figure 1. Top panel: *Swift*/BAT light curve of the 2016 outburst of SMC X-3. The BAT count rate is in units of counts s^{-1} $detector^{-1}$ as reported by the BAT Transient Monitor (Krimm et al. 2013). Bottom panel: *Swift*/XRT light curve of the 2016 outburst of SMC X-3. The XRT flux is in units of erg s^{-1} cm^{-2} in the 0.5–10 keV range and has been calculated from spectral fitting of each observation. The error bars are 1 σ in both panels.

was previously estimated by Klus et al. (2014), based on the long-term spin period evolution of the neutron star. Those results are broadly consistent with the value found in Tsygankov et al. (2017).

In Section 2, we present the *Swift* X-ray observations of the outburst between 2016 July 30 and 2016 December 18 and historical *RXTE* measurements of the long-term spin period. In Section 3, we present the optical photometric and spectroscopic observations. The model used to determine the binary solution and mass accretion rate is described in Section 4 and in Section 5 we discuss the significance of this outburst and draw together our conclusions based on the combined optical and X-ray activity.

2 X-RAY OBSERVATIONS

In this section, we present the *Swift* BAT and XRT light curves and XRT timing of the 2016 super-Eddington outburst of SMC X-3. The *Swift* timing information is compared to the *RXTE* long-term spin period history.

2.1 Swift

The *Swift*/XRT began observing the X-ray outburst of SMC X-3 on 2016 July 30 and continued to detect emission over 5 months later. We present data up to 2016 December 18, which are summarized in the Appendix. Fig. 1 shows the combined BAT and XRT light curves during the outburst. The BAT light curve shown in the top panel is as reported by the BAT Transient Monitor (Krimm et al. 2013). The XRT fluxes shown in the bottom panel were found using time-resolved spectral fitting to individual XRT observations listed in the Appendix.

XRT data were analysed utilizing the HEASOFT V6.19 and the latest XRT calibration files (CALDB 20160609). All XRT data were reprocessed with the standard XRTPIPELINE software, with exposure maps generated in order to compensate for the presence of hot-columns. In order to avoid issues of pile-up, and to use data which has sufficient timing resolution to detect pulsations, we use only data taken in Windowed Timing (WT) mode, in the energy range of 0.5–10 keV. In addition, to avoid issues of event redistribution, we

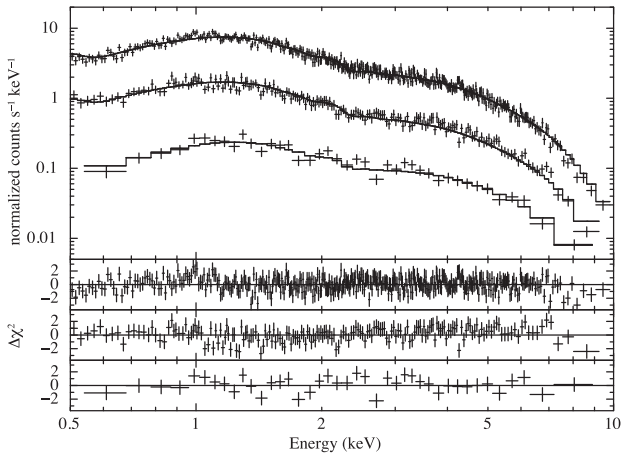

Figure 2. Swift/XRT spectral fits at different flux levels from three epochs of the SMC X-3 outburst. These data are fit with a simple absorbed power-law model, with a low absorption column ($N_{\rm H} \simeq 6.1 \times 10^{20}$ cm^{-2}). In order of decreasing flux, the dates of these observations are 2016 August 20, 2016 October 9 and 2016 December 12. These spectra are binned to have a minimum of 50 counts per bin, the power-law model fits in all cases with a reduced $\chi^2 \simeq 1$. No additional model components are required to describe the XRT data at any point during the period of outburst covered in this paper, there is no evidence of any thermal component.

only utilize WT events of grade 0 for our spectral analysis. Events were extracted from a region of radius 20 pixels around the optical position of SMC X-3, with a background taken from an annulus between 90 and 110 pixels away from the central region, in order to ensure the smallest contamination from SMC X-3 itself.

After careful handing of issues of calibration, pile-up and background subtraction, we found that the XRT spectra throughout the reported outburst period can be well described by a single power-law model, with more complex models not being statistically required. Although no other components are required to fit the spectrum, SMC X-3 does show spectral variability over the outburst, with the photon index averaging $\Gamma \sim 1.08$ during the brightest part of the outburst, and hardening to an average of $\Gamma \sim 0.85$ after MJD 57700. Fig. 2 shows spectral fits of XRT WT data at epochs representing three different flux levels, all well fit by a simple power-law model. This power-law model was used to calculate both the fluxes shown in Fig. 1 and luminosities used in modelling the expected accretion driven spin-up in Section 4. Fluxes were obtained utilizing the XSPEC `cflux` model component for the range of 0.5–10 keV.

We note that the analysis of WT data can be complex due to issues with correctly subtracting the background, in light of the compressed 1-D nature of the data. Incorrect subtraction of the background can often lead to the appearance of a false soft component in the data, which would become more dominant as SMC X-3 fades. The presence of hot columns that are masked out in XRT data further complicates background subtraction, as failing to compensate for this can lead to an oversubtraction of background. In addition, the issue of event redistribution can cause a false soft component if the incorrect or out-of-date calibration files are used.[1] As event redistribution tends to occur mainly in higher grade events, this issue can be mostly avoided by not using WT grade 1 and 2 events. False soft components have often been mistaken as a thermal component in low-mass X-ray binary (LMXB) systems. We suspect that one of these issues is the source of the thermal excess reported in Weng et al. (2017), as we find no evidence of it in our analysis. Furthermore, we suspect the reported soft component seen in EPIC-pn timing mode data on SMC X-3 (Weng et al. 2017) may be incorrect due to known issues of calibration of that mode at low energies (e.g. Pintore et al. 2014).

The power-law index and absorption are typical for X-ray binaries in the SMC and do not show anything abnormal during this giant outburst. Using the flux from the spectral fits, we estimate the outburst reached a peak luminosity of 1.16×10^{39} erg s^{-1} (0.5–10 keV), assuming a source distance of 62 kpc[2] (Scowcroft et al. 2016 and references therein). This is above the Eddington limit for a 1.4 $M_\odot$ neutron star by a factor of roughly 6. As can be seen in Fig. 1, SMC X-3 underwent a rapid increase in flux, before plateauing briefly at this super-Eddington luminosity and entering a phase of more gradual decline.

For the timing analysis, we used event data which were barycentrically corrected using the standard `barycorr` command. Period searches were performed utilizing time tagged events from WT data, which have a time resolution of 1.7791 ms. Each observation made with the XRT in WT mode was run through a timing analysis pipeline to search for the spin period of the neutron star. The period was determined using a standard Rayleighs Z^2_N search (Buccheri et al. 1983), searching a period space around the known 7.78 s period of the source at a resolution of 10^{-6} s. As the pulse profile for SMC X-3 is double peaked, and close to sinusoidal, we found that performing a Z^2_N search with $N = 2$ was sufficient.

Error estimation was performed using the Monte Carlo method of Gotthelf, Vasisht & Dotani (1999), where the folded pulse profile is fitted at the determined frequency and then used to generate 500 simulated event files with Poissonian statistics, utilizing the same observing windows and exposures as the real observations, on which an identical period search is performed again. The error is then calculated by fitting a Gaussian model to the distribution of the fitted periods found from these faked data sets.

The accuracy of *Swift*/XRT timing utilizing these data has been accurately verified by (Cusumano et al. 2012). The Monte Carlo simulations generate event files that exactly mimic the format, time resolution and sampling rate of WT events in real data, with an assumption that the pulse profile and the DC level of the source does not vary significantly across the observation. Given that the observations are typically short, we believe that this is a reasonable approximation. However, if the approximation is not true, it is likely that the effect of this would be to underestimate the error on the period. In all simulations, the simulated histogram of periods was found to be distributed in a Gaussian fashion. All period searching (on real and simulated data) is done with a fixed period resolution (1×10^{-6} s), which was chosen as it is both adequate to sample for Doppler shifts and because the error on each measurement is typically at least an order of magnitude larger. There is no evidence of any red-noise effects due to how we sample the data, real or simulated.

2.2 *RXTE*

The position of SMC X-3 was observed by *RXTE* on a roughly weekly basis between 1999 and the end of the mission in 2012. As

[1] http://www.swift.ac.uk/analysis/xrt/digest_cal.php#abs

[2] Scowcroft et al. (2016) showed that the line-of-sight depth across the SMC varies around the average from −10 kpc in the East, to +10 kpc in the West. SMC X-3 lies roughly in the centre of this distribution and is therefore less likely to be at a significantly different distance than the average value.

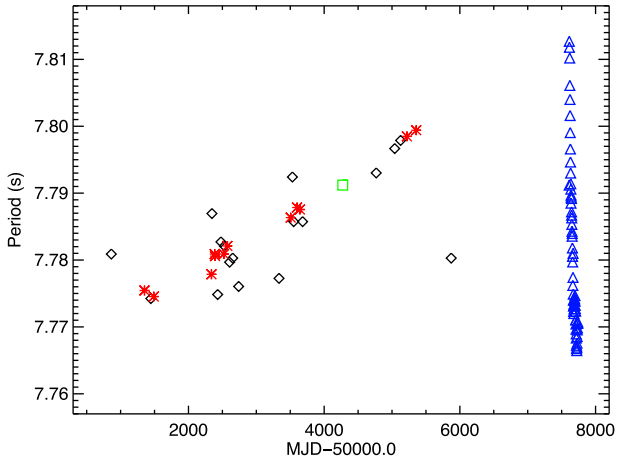

Figure 3. X-ray derived pulsed period history of SMC X-3. Black diamonds and red stars denote *RXTE* period detections above the 99 and 99.99 per cent confidence levels, respectively. Blue triangles denote *Swift* detections of the pulse period during the current outburst. A single *XMM–Newton* detection at MJD 54274 was found in the literature and is denoted by a green square.

described in Section 1, the eventual detection of a 7.78 s period by *RXTE* in 2002 led to the discovery that the known X-ray source, SMC X-3, was an accreting neutron star. In Fig. 3, we show the full spin period history of SMC X-3 as seen by *RXTE*. This figure is an extension of the spin period panel of fig. 7 in Galache et al. (2008). The period measurements were calculated from individual exposures of the *RXTE*/PCA using a Lomb–Scargle analysis method. Because of the large field of view and non-imaging of the PCA, we use the method described in Galache et al. (2008) to subtract out each detected periodicity from the periodogram before searching for the next. The periodogram is searched for known and unknown periods by performing a global period search and smaller searches in a range around a known pulsar period. The detections of SMC X-3 shown in Fig. 3 were found using this search method. More details of this analysis can be found in Galache et al. (2008). In addition, we have included the period detections made by *Swift* during the current giant outburst and a single *XMM–Newton* period measurement found in the literature (Haberl, Eger & Pietsch 2008). One can see the obvious difference between the historical spin period evolution and the evolution during the giant outburst. This is discussed further in Section 5.

3 OPTICAL OBSERVATIONS

In this section, we present optical photometry from the Optical Gravitational Lensing Experiment (OGLE) and optical spectroscopy from the Southern African Large Telescope (SALT) and South African Astronomical Observatory (SAAO) 1.9 m telescope in South Africa, and the European Southern Observatory (ESO) 3.6 m telescope and New Technology Telescope (NTT) in Chile. We use the data to provide the most precise optical period measurement to date and show the evolution of the circumstellar disc over a long baseline, linking this to the X-ray activity in this system.

3.1 OGLE photometry

SMC X-3 was observed during the third and fourth phases of the OGLE project, which has been taking *V*- and *I*-band images with the 1.3 m Warsaw telescope at the Las Campanas Observatory, Chile for the past 20 yr (Udalski et al. 2008; Udalski, Szymański & Szymański 2015). The cadence of observations vary from a few days to roughly a week in the *I* band and slightly longer in the *V* band. The *I* band is a much better tracer of the circumstellar disc in BeXRB systems and, being of high cadence, it is ideal to show the optical variability in SMC X-3. The full 14 yr OGLE light curve of SMC X-3 is shown in the top panel of Fig. 4. The black curve shows the combined OGLE III and IV data, whilst the red curve shows this light curve detrended with a 101 d sliding window function to remove the longer term aperiodic variability, likely caused by changes in the size of the Be star disc. We manually removed the large outburst at the end of the light curve before detrending. The periodic modulations that can be seen throughout both light curves as regular spikes are typically thought to represent the orbital period of the system, though it is becoming clearer that this may not be entirely accurate (see Discussion section). A large 0.4 mag jump in flux near the end of the light curve coincides with the current giant X-ray outburst. It is likely that a sudden growth in the disc has caused this and triggered extensive accretion on to the orbiting neutron star. The optical outburst began on or just after MJD 57601, approximately 2 d after the first X-ray detection by *Swift*, though it is difficult to determine the precise onset due to the cadence of the light curve as well as the aforementioned uncertainty in the onset of the X-ray outburst.

The lower-left panel of Fig. 4 shows the Lomb–Scargle periodogram of the detrended light curve. Overplotted in dashed red lines are the 90, 99, 99.99 and 99.9999 per cent confidence levels, computed directly from the power spectrum statistics. Most of the power is seen at a period of 44.918 ± 0.009 d, which agrees well with the optical value determined by Schmidtke et al. (2013) and the X-ray value determined by Galache et al. (2008). The uncertainty is calculated based on the formula for the standard deviation of the frequency given in Horne & Baliunas (1986). The first harmonic of the fundamental period is easily seen at 22.46 d. Higher order harmonics are also detected down to the sixth harmonic around 6.40 d. This results in quite a complex orbital profile (lower-right panel of Fig. 4). The OGLE III and IV light curves were folded separately and plotted for comparison. One can see that there is very little difference between the two phases, indicating that the period is very stable over more than a decade of observations. The profiles are also highly skewed in a 'fast rise, exponential decay' shape. This shape is indicative of the modulation being related to the binary period of the system (e.g. Bird et al. 2012). The ephemeris of peak flux is MJD 57682.14 ± 0.37. This will be discussed further in Section 5 in the context of the orbital ephemeris from binary model fitting.

3.2 Spectroscopy

Observations were obtained from the SALT and SAAO 1.9 m telescopes just after the peak of the X-ray outburst to measure the shape and equivalent width of the H_α emission line and to see if any other features were present. These were compared with several archival spectra from the SAAO 1.9 m and ESO 3.6 m and NTT telescopes obtained sporadically over the past ∼20 yr. The details of these observations, and the measured equivalent widths, are shown in Table 1.

Fig. 5 shows the H_α equivalent width measurement from each of the archival spectra obtained with the SAAO 1.9 m telescope and the ESO 3.6 m and NTT telescopes, as well as the SAAO 1.9 m and SALT/RSS spectra taken during the current outburst. Despite large gaps in the coverage of SMC X-3, there is moderate evidence that the circumstellar disc around the Be star has grown in recent months; as suggested by the OGLE photometry. However, there is also evidence

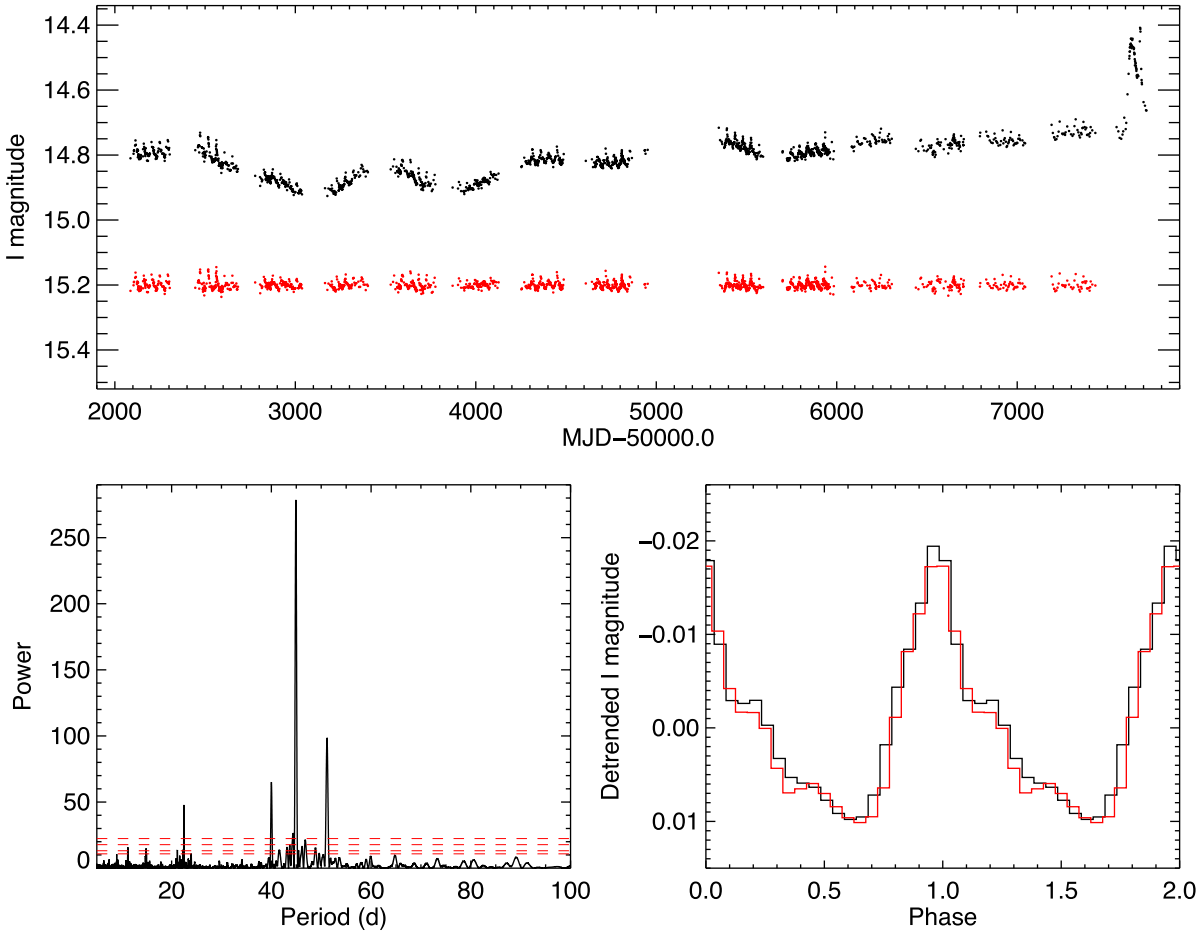

Figure 4. Top panel: OGLE III and IV light curve of SMC X-3 in the *I* band (black). The detrended light curve is shown for comparison (red). For clarity, 15.2 mag have been added to the detrended light curve. Bottom-left panel: Lomb–Scargle periodogram of the detrended OGLE light curve, excluding the recent outburst. The most prominent peak corresponds to a period of 44.918 d. The next highest peaks at periods of 40.00 d and 51.16 d are attributed to aliasing. There are smaller peaks visible, corresponding to harmonics of the main period. The dashed red lines are the 90, 99, 99.99 and 99.9999 per cent confidence levels. Bottom-right panel: the detrended OGLE light curve folded at the 44.918 d period. OGLE III is in black and OGLE IV in red.

Table 1. Observation time, telescope and equivalent width of each spectrum used in our analysis.

Date	MJD	Telescope	H_α EW
2001 November 11	52224	SAAO 1.9 m	−11.4 ± 0.5
2003 November 6	52949	SAAO 1.9 m	−12.1 ± 0.7
2005 October 27	53670	SAAO 1.9 m	−11.8 ± 1.0
2006 November 10	54049	SAAO 1.9 m	−10.2 ± 0.4
2007 September 17	54360	ESO 3.6 m	−11.7 ± 0.3
2011 December 11	55906	NTT	−12.4 ± 0.2
2016 September 4	57635	SAAO 1.9 m	−13.5 ± 0.7
2016 September 6	57637	SAAO 1.9 m	−12.7 ± 0.6
2016 September 6	57637	SALT	−11.5 ± 0.1
2016 September 11	57642	SALT	−11.0 ± 0.1
2016 November 13	57705	SALT	−13.4 ± 0.1
2016 November 25	57717	SAAO 1.9 m	−15.5 ± 0.4

for rapid variability in the line emission that is unexpected in this type of binary system, even during a large outburst. This point is discussed in Section 5.

In addition to these data, we obtained a blue SALT/RSS spectrum to look for the presence of helium in emission. We compare this spectrum to an ESO 3.6 m spectrum obtained in 2006 September (see McBride et al. 2008 for a description of the ESO observation

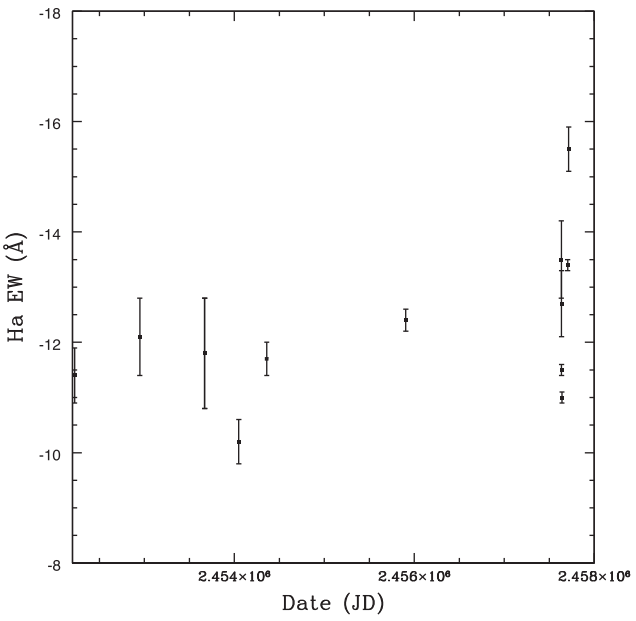

Figure 5. Measured values of the H_α equivalent width from the spectra listed in Table 1.

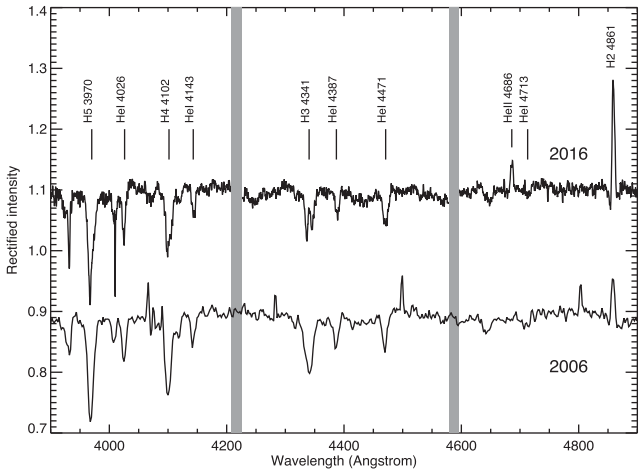

Figure 6. ESO 3.6 m spectrum from 2006 and SALT RSS spectrum taken during the current X-ray outburst. The spectra are rectified and offset from 1.0 by 0.1 on either side for clarity. The vertical grey lines represent the chip gaps in the SALT CCD.

and the data reduction). The blue SALT/RSS spectrum was obtained using the PG2300 grating at an angle of 30.5 deg, yielding a resolution of 2.1 Å. Fig. 6 shows the archival ESO spectrum and the recent SALT spectrum taken during the outburst. He II 4686 is clearly in emission during the outburst and not present in the archival spectrum (MJD 53993), which was taken during X-ray quiescence as shown by the lack of X-ray pulsations detected in *RXTE* observations on MJD 53992 and 53998 (see also Fig. 3). This is likely evidence of a transient accretion disc around the neutron star. The H_β line shows evidence of a very narrow emission component superimposed on a rotationally broadened absorption line, typical of many early-type emission line stars. The emission component is also stronger than it was in 2006. Emission in H_γ and possibly H_δ is also apparent in the 2016 SALT spectrum. This is further good evidence that the disc has grown in the time between these observations.

4 ORBITAL SOLUTION

The measured pulsar period of SMC X-3 shows significant variability during the outburst, overall showing a decrease in period due to pulsar spin-up, but also showing modulation due to Doppler shift caused by orbital motion. We attempted to model the evolution of the pulsar period utilizing several models. First, we fit the data with a model comprising of a simple spin-up (i.e. constant $\dot{P}$), with orbital modulation. Unfortunately we were not able to obtain an adequate fit to the data utilizing this model, suggesting that the spin-up of the pulsar was not linear.

In an attempt to model this, we followed the example of Takagi et al. (2016) which modelled $\dot{P}$ utilizing the equation of Ghosh & Lamb (1979), which suggests that the spin-up of a pulsar is proportional to $L_{37}^{6/7}$, where L_{37} is the bolometric luminosity of the pulsar in units of 10^{37} erg s^{-1}. We simplified this by assuming that all the values other than L_{37} and P in equation 3 of Takagi et al. (2016) can be combined into a constant. Note that for L_{37} we simply use a model-fitted luminosity based on the spectral fitting described in Section 2 and corrected for a standard SMC distance of 62 kpc. We assume that the correction from this luminosity to a bolometric luminosity is constant, and include that in the fitted constant parameter. Therefore, the fitted model becomes:

$$\dot{P} = C \times P^2 \times L_{37}(0.5 - 10\ \mathrm{keV})^{6/7} \quad (1)$$

Fitting this model, including an orbital Doppler shift as detailed in Coe et al. (2015), to our data provides a much improved fit over a simple linear $\dot{P}$, however the model underestimates the spin-up in the latter parts of the outburst. In order to compensate for this, we attempted three variations of the model. First, we added in an additional $\dot{P}$ value to account for the poor fit in the latter parts of the outburst. Secondly, we allowed the luminosity index in equation (1) to be a fitted parameter. Thirdly, we fit the model with a variable luminosity index and $\dot{P}$, which resulted in the best-fitting solution as shown in Fig. 7 and Table 2. We stress that this model is simply a parametrization of the data and does not represent a realistic model explaining the spin period evolution. However, in fitting the underlying period evolution like this, it allows us to accurately determine the orbital parameters of the system. It is apparent that the model struggles to fit the data where there are sharp or complex changes in the spin period (e.g. near MJD 57675), which are likely due to some higher order spin variability that is difficult or impossible to model. Indeed, Ghosh & Lamb (1979) assume accretion is from an aligned disc, whereas in reality the accretion in a BeXRB is likely to be more complex than this, which may affect the relationship. The assumption that the correction from XRT flux to bolometric flux is a constant throughout the outburst is also likely not entirely accurate, given that the spectral parameters are seen to vary throughout the outburst.

In order to test whether our binary model does reliably determine the orbital parameters in this system, we applied a simple $\dot{P} + \ddot{P}$ model to the data that does not take into account the luminosity of the outburst. This removes the uncertainty arising from our assumption of a constant bolometric flux correction, but means that rapid changes in the spin period are less likely to be accounted for than in the previous model. Indeed, this proved to be the case as the model was unable to converge to a physically realistic set of parameters. We applied the same model to a subset of the data that excluded the initial super-Eddington part of the outburst, resulting in a much improved fit. This may be due to more complex spin period variability being present during the onset of the outburst, or because the errors on our spin period measurements are being underestimated at higher luminosities due to an imperfect model of the shape of the pulse profile. The result is marginally consistent with the solution in Table 2 (3σ), albeit with larger errors, and confirms that we are reliably extracting the true binary parameters in the full model.

5 DISCUSSION

At the time of writing, SMC X-3 was still being detected at a high level of confidence with *Swift* having been in X-ray outburst for 5 months. It is one of the longest and brightest outbursts ever recorded from a BeXRB. We discuss the results of our observations and compare SMC X-3 to the known population of BeXRBs.

5.1 Neutron star spin

Fig. 3 shows that the general spin-down trend observed in this system by Galache et al. (2008) continued through the latter stages of *RXTE* monitoring, right up to the start of the current giant outburst on MJD 57599. At this point we detect significant spin-up, unlike anything observed in this system before. The spin period measured at the time of writing is lower than the very first measurement by *RXTE*, showing that the momentum transferred by material accreted during the last 5 months has been greater than the momentum lost by magnetic breaking over the past 18 yr. Klus et al. (2014) measure the long-term spin-down of SMC X-3 to

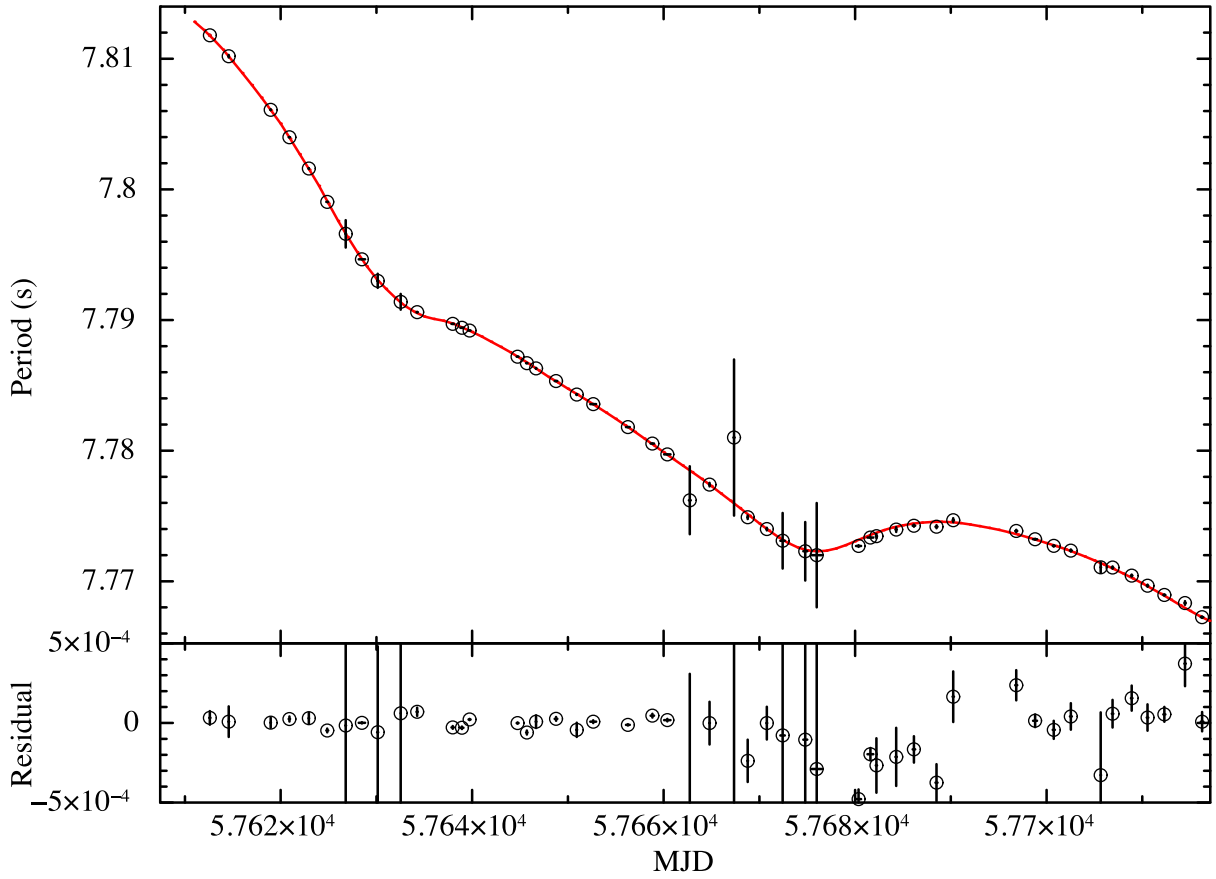

Figure 7. Top panel: *Swift* period measurements with the combined binary and spin-up model overplotted in red. Note that the fitted parameters for this model are given in Table 2. Lower panel: residuals of the fit.

be $0.00262 \pm 0.00003\,\mathrm{s\,yr^{-1}}$ and the average luminosity (during outburst) to be $(3.6 \pm 0.1) \times 10^{36}\,\mathrm{erg\,s^{-1}}$. This value is roughly 500 times lower than the spin-*up* value of $\sim -0.13\,\mathrm{s\,yr^{-1}}$ seen during the current outburst, showing the significantly larger torques present during this outburst. Even during previous Type I outbursts recorded by *RXTE*, the spin period seems to continue increasing under low levels of accretion. This is probably evidence of extremely efficient accretion from a transient accretion disc in the current giant outburst.

5.2 System parameters and mass function

In trying to model the binary orbit of SMC X-3, we were using a data set containing incredibly complex variations in the measured neutron star spin period. Thus, it was very difficult to properly account for the whole outburst without modifying certain accretion models or taking subsets of the data. The reason for not fixing the binary period at the very precise value determined from the optical light curve, is because of the growing evidence that this optical period does not necessarily represent the exact binary period (e.g. Bird et al. 2012; Vasilopoulos et al. 2014). Whilst in this case we have shown that the periods are consistent at the 2σ level, we cannot be certain enough that they are exactly the same to fix the parameter in the final fit. In addition, our binary parameters in Table 2 are entirely consistent with those found by Tsygankov et al. (2017) using a similar method, but show slight differences to those of Weng et al. (2017) not consistent within errors.

Table 2. Binary solution obtained in this work.

Parameter		Value
Orbital period	P_{orbital} (d)	45.04 ± 0.08
Projected semimajor axis	$a_x \sin i$ (light-s)	190.3 ± 1.3
Longitude of periastron	ω (^{o})	204.3 ± 1.1
Eccentricity	e	0.244 ± 0.005
Orbital epoch	τ_{per} (MJD)	57676.4 ± 0.2
GL79 index (c.f. 0.857)	GL79 index	0.61 ± 0.01
First derivative of P	$\dot{P}$ (10^{-10} ss^{-1})	-7.4 ± 0.8
Goodness of fit	χ^2_ν (degrees of freedom)	321 (54)

The binary parameters are known in seven other BeXRB systems in the SMC (Townsend et al. 2011; Coe et al. 2015). When compared to this group, SMC X-3 seems to have a lower than expected eccentricity for its orbital period, sitting in between the 'normal' BeXRB systems and the group of low eccentricity systems suggested by Pfahl et al. (2002) in fig. 6 of Townsend et al. (2011). Thus, we may be starting to see evidence that these systems are formed from supernovae with a broad continuum of kick amplitudes, instead of the discrete 'large' or 'small' kick scenario, which results in a broad range of eccentricities and orbital periods. SMC X-3 also has the highest measured projected semimajor axis of the SMC systems to date, despite having a low eccentricity. The mass function derived from these parameters is $3.7\,\mathrm{M}_\odot$, typical of other BeXRBs.

5.3 Circumstellar disc

The stable and highly significant periodicity measured in the OGLE light curve is consistent with the binary period in Table 2 to within 2σ. This period is also seen in the long-term *RXTE* light curve (Galache et al. 2008), making it probable that the optical period represents the binary period. We find an ephemeris of maximum optical flux of MJD 57682.14 $\pm$ 0.37, whereas the dynamically determined orbital ephemeris is MJD 57676.4 $\pm$ 0.2. This suggests that the peak in optical flux occurs roughly 6 d after periastron, and that this offset is stable over more than a decade. Smoothed-Particle Hydrodynamic (SPH) simulations (Okazaki et al. 2002) show that for any non-zero eccentricity the neutron star distorts the disc shape as it goes through periastron. This distortion increases the surface area of the circumstellar disc leading to an optical flare or enhancement. A lag of $\sim$6 d is an indication of how long this process takes, probably related to the disc viscosity. This effect is observed in other well-known systems, such as PSR B1259–63. The ephemeris derived from the *RXTE* light curve is not precise enough to extrapolate forward and compare to the other ephemerides, so we do not know whether the maximum in X-ray flux occurs at periastron or not.

The OGLE light curve and the historical H_α measurements suggest the disc in SMC X-3 has been very stable over more than a decade. Some of the Be stars in BeXRBs do exhibit this behaviour, though it is more common to see some large-scale variability on time-scales of a few years.[3] The increase in optical flux coincides with the X-ray outburst, meaning the circumstellar disc is the source of extra material for this outburst, though the brightening of 0.3 mag is still only a moderate rise given the enormity of the X-ray outburst. The consistently single peaked H_α emission seems to point towards a disc that is not highly inclined to our line of sight, meaning a large increase in the size of the disc is not being hidden from us by a projected inclination effect.

Spectroscopic coverage of SMC X-3 has been sparse, making it hard to say whether the disc emission in H_α mimics the long-term broad-band optical emission. However, we have observed the H_α emission to be variable on shorter time-scales, not seen in the optical light curve. Fig. 8 shows the measured H_α emission during the outburst and the corresponding *I*-band flux during this time. One can see that the H_α emission changes by at least 1 Å in a matter of hours and by as much as 50 per cent in a few days. This variability is not reflected in the *I*-band flux. To check that the errors are not being underestimated, we measured the equivalent widths in several different ways: Gaussian fitting, randomized continuum fitting using a Monte Carlo method and using the STARLINK/DIPSO software, where the errors are calculated using the prescriptions given by Howarth & Phillips (1986). In all cases, the error bars were similar and confirmed the variability must be intrinsic to the source. Unfortunately, the coverage around any given orbit of the neutron star is not sufficient to say if this is linked to orbital phase in some way. The cause could be the interaction of the neutron star with inhomogeneities in the expanded disc, but this is difficult to confirm given these data.

6 CONCLUSIONS

This paper presents X-ray and optical observations made between 2016 July 30 and 2016 December 18 during the first 5 months of the giant X-ray outburst of SMC X-3. The peak X-ray luminosity is far in excess of the Eddington limit for a canonical mass neutron star, making it a nearby ultraluminous X-ray source. The complex period changes, likely caused by variable accretion torques, have been untangled from the orbital modulations allowing us to measure the binary parameters. We show the binary parameters of this system are typical of other BeXRB systems, though perhaps somewhat on the edge of the distribution of eccentricities of 'normal' BeXRB systems given the longer binary period. When compared to historical spin period measurements made by *RXTE*, the pulsar is seen to deviate from a state of constant spin-down to an extremely rapid spin-up that returned the neutron star spin period to that observed 18 yr ago, in just 5 months.

The optical period of 44.918 d is consistent with the dynamically determined binary period and the long-term X-ray period within errors. However, the ephemeris shows the optical emission is delayed by around 6 d from periastron, which may be linked to viscous time-scales in the disc as it is being distorted by the neutron star. The H_α emission from the disc is variable on short time-scales which may be linked to the disc being inhomogeneous or time-variable, though the data are not sufficient to confirm this hypothesis. We also observe He II in emission, showing the reservoir of material is sufficient to fuel a stable accretion disc around the neutron star, reflecting the enormity of this outburst.

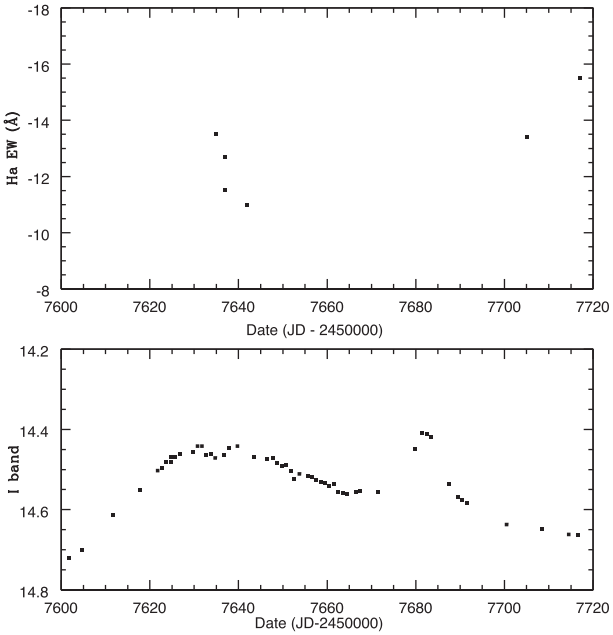

Figure 8. Measured H_α emission during the X-ray outburst of SMC X-3 plotting above the corresponding OGLE *I*-band photometry.

ACKNOWLEDGEMENTS

We thank the anonymous referee for their help in improving this manuscript. We would like to acknowledge Elizabeth Bartlett for providing the NTT spectrum included in our analysis. LJT is supported by the University of Cape Town Research Committee. JAK acknowledges the support of NASA grant NNX15AR44G through the Swift GI program. VAM and DAHB acknowledge support from the South African National Research Foundation. Some of these observations were obtained with the Southern African Large Telescope under program 2016-2-MLT-010. The OGLE project has received funding from the National Science Centre, Poland, grant MAESTRO 2014/14/A/ST9/00121 to AU.

[3] See the OGLE XROM data analysis system (Udalski 2008) for long-term light curves of most BeXRBs in the SMC.

REFERENCES

Antoniou V., Zezas A., Hatzidimitriou D., Kalogera V., 2010, ApJ, 716, L140
Bird A. J., Coe M. J., McBride V. A., Udalski A., 2012, MNRAS, 423, 3663
Buccheri R. et al., 1983, A&A, 128, 245
Casares J., Negueruela I., Ribó M., Ribas I., Paredes J. M., Herrero A., Simón-Díaz S., 2014, Nature, 505, 378
Clark G., Doxsey R., Li F., Jernigan J. G., van Paradijs J., 1978, ApJ, 221, L37
Coe M. J., Kirk J., 2015, MNRAS, 452, 969
Coe M. J., Bartlett E. S., Bird A. J., Haberl F., Kennea J. A., McBride V. A., Townsend L. J., Udalski A., 2015, MNRAS, 447, 2387
Corbet R. H. D., Edge W. R. T., Laycock S., Coe M. J., Markwardt C. B., Marshall F. E., 2003, in AAS/High Energy Astrophysics Division #7. p. 629
Cowley A. P., Schmidtke P. C., 2004, AJ, 128, 709
Crampton D., Hutchings J. B., Cowley A. P., 1978, ApJ, 223, L79
Cusumano G. et al., 2012, A&A, 548, A28
Dray L. M., 2006, MNRAS, 370, 2079
Edge W. R. T., 2005, PhD thesis, University of Southampton (United Kingdom), 6
Edge W. R. T., Coe M. J., Corbet R. H. D., Markwardt C. B., Laycock S., 2004, Astron. Telegram, 225
Galache J. L., Corbet R. H. D., Coe M. J., Laycock S., Schurch M. P. E., Markwardt C., Marshall F. E., Lochner J., 2008, ApJS, 177, 189
Ghosh P., Lamb F. K., 1979, ApJ, 234, 296
Gotthelf E. V., Vasisht G., Dotani T., 1999, ApJ, 522, L49
Haberl F., Sturm R., 2016, A&A, 586, A81
Haberl F., Eger P., Pietsch W., 2008, A&A, 489, 327
Horne J. H., Baliunas S. L., 1986, ApJ, 302, 757
Howarth I. D., Phillips A. P., 1986, MNRAS, 222, 809
Kennea J. A. et al., 2016, Astron. Telegram, 9362
Klus H., Ho W. C. G., Coe M. J., Corbet R. H. D., Townsend L. J., 2014, MNRAS, 437, 3863
Krimm H. A. et al., 2013, ApJS, 209, 14
Li F., Jernigan G., Clark G., 1977, IAU Circ., 3125
McBride V. A., Coe M. J., Negueruela I., Schurch M. P. E., McGowan K. E., 2008, MNRAS, 388, 1198
Negoro H. et al., 2016, Astron. Telegram, 9348
Okazaki A. T., Bate M. R., Ogilvie G. I., Pringle J. E., 2002, MNRAS, 337, 967
Pfahl E., Rappaport S., Podsiadlowski P., Spruit H., 2002, ApJ, 574, 364
Pintore F. et al., 2014, MNRAS, 445, 3745
Reig P., 2011, Ap&SS, 332, 1
Schmidtke P. C., Cowley A. P., Udalski A., 2013, MNRAS, 431, 252
Scowcroft V., Freedman W. L., Madore B. F., Monson A., Persson S. E., Rich J., Seibert M., Rigby J. R., 2016, ApJ, 816, 49
Takagi T., Mihara T., Sugizaki M., Makishima K., Morii M., 2016, PASJ, 68, S13
Townsend L. J., Coe M. J., Corbet R. H. D., Hill A. B., 2011, MNRAS, 416, 1556
Tsygankov S. S., Doroshenko V., Lutovinov A. A., Mushtukov A. A., Poutanen J., 2017, A&A, preprint (arXiv:1702.00966)
Udalski A., 2008, AcA, 58, 187
Udalski A., Szymanski M. K., Soszynski I., Poleski R., 2008, AcA, 58, 69
Udalski A., Szymański M. K., Szymański G., 2015, AcA, 65, 1
van Paradijs J., Schlosser W., Tarenghi M., Sanduleak N., Philip A. G. D., 1977, IAU Circ., 3134
Vasilopoulos G., Haberl F., Sturm R., Maggi P., Udalski A., 2014, A&A, 567, A129
Vasilopoulos G., Haberl F., Antoniou V., Zezas A., 2016, Astron. Telegram, 9229
Walter R., Lutovinov A. A., Bozzo E., Tsygankov S. S., 2015, A&A Rev., 23, 2
Weng S.-S., Ge M.-Y., Zhao H.-H., Wang W., Zhang S.-N., Bian W.-H., Yuan Q.-R., 2017, ApJ, 843, 69

APPENDIX A: DETAILS OF *SWIFT* OBSERVATIONS

Table A1 presents the OBSID, exposure time, measured luminosity and measured spin period for each *Swift* observation used in this work.

Table A1. *Swift* observations used in this work.

ObsID	T_{START} (MJD)	T_{STOP} (MJD)	Exposure (s)	0.5–10 keV luminosity (10^{38} erg s^{-1})	Period (s)
00034673001	57610.93	57611.07	4658	$3.85^{+0.05}_{-0.05}$	–
00034673001	57611.00	57611.00	75	$0.33^{+0.26}_{-0.17}$	–
00034673002	57612.53	57612.66	1971	$4.72^{+0.08}_{-0.08}$	7.811800 ± 0.000043
00034673003	57614.53	57614.60	932	$6.38^{+0.14}_{-0.14}$	7.810200 ± 0.000096
00034673004	57618.91	57618.98	1993	$6.69^{+0.08}_{-0.08}$	7.806100 ± 0.000032
00034673005	57620.84	57620.98	2044	$8.77^{+0.12}_{-0.12}$	7.804000 ± 0.000016
00034673006	57622.90	57622.97	1953	$9.00^{+0.10}_{-0.10}$	7.801600 ± 0.000036
00034673007	57624.76	57624.96	1287	$11.44^{+0.15}_{-0.15}$	7.799046 ± 0.000012
00034673008	57626.75	57626.82	503	$10.30^{+0.22}_{-0.22}$	7.796600 ± 0.001049
00034673009	57628.15	57628.81	1578	$10.43^{+0.13}_{-0.13}$	7.794653 ± 0.000004
00034673010	57630.07	57630.19	795	$9.76^{+0.18}_{-0.17}$	7.793000 ± 0.000540
00034673011	57632.52	57632.53	792	$10.81^{+0.21}_{-0.21}$	7.791400 ± 0.000605
00034673012	57634.19	57634.32	1925	$8.46^{+0.12}_{-0.11}$	7.790600 ± 0.000026
00034673013	57636.17	57636.64	1339	$5.15^{+0.10}_{-0.10}$	7.788500 ± 0.000777
00034673014	57637.83	57638.09	2974	$5.97^{+0.06}_{-0.06}$	7.789706 ± 0.000009
00034673015	57638.76	57639.09	2963	$6.62^{+0.08}_{-0.08}$	7.789408 ± 0.000008
00034673016	57639.62	57639.83	2756	$5.63^{+0.07}_{-0.07}$	7.789200 ± 0.000004
00034673017	57644.64	57644.85	2966	$4.83^{+0.06}_{-0.06}$	7.787200 ± 0.000004
00034673018	57645.63	57645.78	2973	$4.54^{+0.06}_{-0.06}$	7.786700 ± 0.000013
00034673019	57646.63	57646.71	2975	$4.67^{+0.06}_{-0.06}$	7.786300 ± 0.000040

Table A1 – *continued*

ObsID	T_{START} (MJD)	T_{STOP} (MJD)	Exposure (s)	0.5–10 keV luminosity (10^{38} erg s^{-1})	Period (s)
00034673020	57648.62	57648.90	2995	$3.47^{+0.05}_{-0.05}$	7.785329 ± 0.000012
00034673021	57650.87	57650.96	2912	$3.02^{+0.05}_{-0.05}$	7.784300 ± 0.000045
00034673022	57652.33	57652.95	2583	$2.91^{+0.05}_{-0.05}$	7.783560 ± 0.000009
00034673023	57654.01	57654.68	2982	$2.70^{+0.04}_{-0.04}$	7.783964 ± 0.000010
00034673024	57656.06	57656.46	2070	$2.60^{+0.05}_{-0.05}$	7.781800 ± 0.000004
00034673025	57658.64	57659.00	3279	$2.42^{+0.04}_{-0.04}$	7.780547 ± 0.000012
00034673026	57660.05	57660.72	2959	$2.03^{+0.04}_{-0.04}$	7.779710 ± 0.000008
00034673027	57662.63	57662.83	550	$1.61^{+0.09}_{-0.09}$	7.776200 ± 0.002603
00034673028	57664.75	57664.83	1713	$1.62^{+0.05}_{-0.05}$	7.777400 ± 0.000134
00034673029	57667.28	57667.42	723	$1.38^{+0.10}_{-0.09}$	7.781000 ± 0.005977
00034673030	57668.75	57668.82	2783	$1.53^{+0.04}_{-0.04}$	7.774900 ± 0.000133
00034673031	57670.73	57670.81	2833	$1.33^{+0.03}_{-0.03}$	7.774000 ± 0.000103
00034673032	57672.19	57672.66	1976	$1.27^{+0.04}_{-0.04}$	7.773100 ± 0.002129
00034673033	57674.58	57675.00	2020	$1.21^{+0.04}_{-0.04}$	7.772300 ± 0.002243
00034673034	57675.46	57676.52	1195	$1.10^{+0.05}_{-0.05}$	7.772000 ± 0.003997
00034673035	57680.10	57680.63	2483	$1.00^{+0.04}_{-0.03}$	7.772697 ± 0.000061
00034673036	57681.30	57681.90	2844	$0.95^{+0.03}_{-0.03}$	7.773350 ± 0.000039
00034673037	57682.16	57682.29	3426	$0.94^{+0.03}_{-0.03}$	7.773456 ± 0.000171
00034673038	57684.21	57684.36	3677	$0.94^{+0.03}_{-0.03}$	7.773963 ± 0.000183
00034673039	57686.01	57686.28	3615	$0.86^{+0.03}_{-0.03}$	7.774258 ± 0.000083
00034673040	57688.40	57688.61	2939	$0.74^{+0.03}_{-0.03}$	7.774179 ± 0.000116
00034673041	57690.18	57690.33	3976	$0.91^{+0.03}_{-0.03}$	7.774677 ± 0.000159
00034673043	57696.73	57696.94	3963	$0.77^{+0.03}_{-0.03}$	7.773852 ± 0.000095
00034673042	57698.59	57699.00	5241	$0.74^{+0.02}_{-0.02}$	7.773220 ± 0.000040
00034673044	57700.65	57700.86	4636	$0.60^{+0.02}_{-0.02}$	7.772715 ± 0.000057
00034673045	57702.44	57702.64	4441	$0.63^{+0.02}_{-0.02}$	7.772353 ± 0.000083
00034673046	57706.82	57706.97	4439	$0.58^{+0.02}_{-0.02}$	7.771050 ± 0.000087
00034673047	57708.81	57708.97	4318	$0.57^{+0.02}_{-0.02}$	7.770433 ± 0.000079
00034673048	57710.47	57710.62	4617	$0.53^{+0.02}_{-0.02}$	7.769663 ± 0.000083
00034673049	57712.20	57712.41	4869	$0.51^{+0.02}_{-0.02}$	7.768950 ± 0.000047
00034673050	57714.40	57714.54	3278	$0.45^{+0.03}_{-0.02}$	7.768338 ± 0.000142
00034673051	57716.11	57716.39	4472	$0.39^{+0.02}_{-0.02}$	7.767253 ± 0.000061
00034673053	57718.31	57718.46	4421	$0.37^{+0.02}_{-0.02}$	7.766753 ± 0.000096
00034673054	57720.23	57720.45	4578	$0.30^{+0.02}_{-0.02}$	7.766453 ± 0.000082
00034673055	57722.55	57722.77	5014	$0.33^{+0.02}_{-0.02}$	7.766975 ± 0.000084
00034673056	57724.08	57724.30	4552	$0.26^{+0.02}_{-0.02}$	7.767576 ± 0.000060
00034673057	57726.54	57726.76	4903	$0.23^{+0.02}_{-0.02}$	7.768563 ± 0.000081
00034673058	57728.53	57728.75	4906	$0.16^{+0.01}_{-0.01}$	7.769552 ± 0.000079
00034673059	57730.07	57730.48	4513	$0.22^{+0.02}_{-0.02}$	7.769852 ± 0.000071
00034673060	57732.05	57732.20	4700	$0.26^{+0.01}_{-0.01}$	7.770529 ± 0.000095
00034673061	57734.79	57734.98	3064	$0.26^{+0.02}_{-0.02}$	7.770563 ± 0.000108
00034673062	57736.44	57736.72	3529	$0.26^{+0.02}_{-0.02}$	7.770734 ± 0.000071
00034673063	57738.03	57738.31	4367	$0.29^{+0.02}_{-0.02}$	7.770563 ± 0.000050
00034673064	57750.42	57750.96	5024	$0.22^{+0.01}_{-0.01}$	7.768773 ± 0.000027
00034673065	57752.54	57752.74	4279	$0.20^{+0.01}_{-0.01}$	7.768268 ± 0.000120
00034673066	57754.20	57754.41	4493	$0.18^{+0.01}_{-0.01}$	7.767672 ± 0.000116
00034673067	57763.42	57763.96	1484	$0.08^{+0.02}_{-0.02}$	–
00034673069	57766.21	57766.54	1660	$0.04^{+0.01}_{-0.01}$	–
00034673081	57780.10	57780.31	2289	$0.17^{+0.02}_{-0.02}$	–

This paper has been typeset from a TEX/LATEX file prepared by the author.